Volcanic signatures in time gravity variations during the volcanic unrest on El Hierro (Canary Islands)

S. Sainz-Maza[1*)], J. Arnoso[2,4)], F. G. Montesinos[3,4)], J.Martí[5)]

[1)] Observatorio Geofísico Central (IGN). C/ Alfonso XII, 3. 28014 Madrid, Spain.

[2)] Instituto de Geociencias (CSIC, UCM). Facultad de Matemáticas. Plaza de Ciencias, 3. 28040 Madrid, Spain.

[3)] Facultad de Matemáticas. Universidad Complutense de Madrid. Plaza de Ciencias, 3. 28040 Madrid, Spain.

[4)] Grupo Geodesia-UCM, Madrid, Spain.

[5)] Instituto de Ciencias de la Tierra *Jaume Almera* (CSIC). C/ Lluís Solé i Sabarís s/n, 08028 Barcelona, Spain.

*) Corresponding author

Sergio Sainz-Maza

e-mail: ssainz-maza@fomento.es. Tel. +34 915270107 (+0361)

Submitted for publication:

Journal of Geophysical Research (Solid Earth)

Abstract

Gravity changes occurring during the initial stage of the 2011–2012 El Hierro submarine eruption are interpreted in terms of the pre-eruptive signatures during the episode of unrest. Continuous gravity measurements were made at two sites on the island using the relative spring gravimeter LCR gPhone-054. On September 15, 2011, an observed gravity decrease of 45 μGal, associated with the southward migration of seismic epicenters, is consistent with a lateral magma migration occurred beneath the volcanic edifice, an apparently clear precursor of the eruption that took place 25 days later on October 10, 2011. High-frequency gravity signals also appeared on October 6–11, 2011, point to an interaction between a magmatic intrusion and the ocean floor was occurring. These important gravity changes, with amplitudes varying from 10 to -90 μGal, during the first three days following the onset of the eruption are consistent with the northward migration of the eruptive focus along an active eruptive fissure. An apparent correlation of gravity variations with body tide vertical strain was also noted, which could indicate that concurrent tidal triggering occurred during the initial stage of the eruption.

Keywords: El Hierro; continuous gravity; volcanic unrest; submarine eruption; volcanic precursor

1. Introduction

Gravity measurements are usually taken on active volcanoes to monitor their activity, identify the precursory signals of new eruptions, and constrain the nature of unrest [*Rymer and Williams-Jones*, 2000; *Furuya et al*., 2003; *Gottsmann et al*., 2006; *Crescentini et al*., 2007; *Bonafede and Ferrari*, 2009]. Gravity variations caused by volcanic sources can range from one to several hundred μGal (1 μGal = 10^{-8} ms^{-2}) and may occur at any time during phases of volcanic activity [*Bonvalot et al.*, 1998; *Greco et al.*, 2008]. After subtracting the solid-earth and ocean-tide effects (and, likewise, any meteorological/hydrological perturbations) from the gravity records, the corresponding residuals are useful for detecting volcanic signals and as an effective volcano-monitoring tool if combined with other geodetic/geophysical parameters such as seismicity, deformation and geochemical data. Furthermore, time variations in the observed Earth-tide parameters (other than the lunisolar gravitational attraction) could indicate ground deformation processes occurring as a result of volcanic events [*Berrino et al.*, 2006]. Along with certain other observational techniques, the analysis of continuous gravity measurements allows the temporal evolution of volcanic processes to be studied, and can make an important contribution to the investigation of subsurface mass redistributions and density changes, magmatic processes, and changes in elevation and seismicity.

Several studies using continuous gravity measurements have been carried out on different islands of the Canary archipelago since 1987, all with the aim of improving our understanding of the Earth's crustal response to tidal forces in volcanic areas and of gathering gravity signals related to volcanic/seismic activity during periods of quiescence [*Vieira et al.*, 1991; *Arnoso et al.*, 2000; 2001; 2011]. However, to the knowledge of the authors, studies based on continuous gravity variations during an active volcanic process in the Canary Islands had hitherto not been undertaken.

From the onset of seismic activity in July 2011, various geodetic and geophysical parameters were placed under continuous observation on El Hierro. The Spanish IGN implemented a surveillance network consisting of four GPS stations, progressively increased to a total of 12 stations, nine seismic stations (two of which are a permanent part of the volcano IGN monitoring network in the Canary Islands), several geochemical techniques (Radon concentration, CO_2 flux, groundwater parameters) and three magnetometers [*López et al.*, 2012]. A tiltmeter network was also installed to monitor ground deformations [*Arnoso et al.*, 2012], whilst a control gravity network, in place since 2003, was used to study gravity variations in terms of subsurface mass/density changes due to volcanic activity. Additionally,

another GPS network with a total of six stations was installed by the local agency ITER [*Sagiya et al.*, 2012], and also operative was a GPS antenna (FRON), which had been erected by the GRAFCAN (Cartographical Service of the Government of the Canary Islands) in 2010.

To complement this monitoring network we installed a permanent gravimeter to conduct continuous gravity measurements. Time gravity variations associated with seismic-volcanic processes can make a significant contribution to real-time volcano monitoring and, in particular, to the investigation of magma dynamics and subsurface processes during episodes of unrest. The data thus generated can also provide important constraints on the geometry of subsurface structures beneath the volcanic edifice and on the source of unrest. In this paper, we document the continuous gravity measurements carried out on El Hierro during the unrest episode preceding the submarine eruption that occurred in 2011–2012. Although the gravity measurements that began in late July 2011 have continued to the present, we concentrate our study on the period between August 6, 2011 and October 15, 2011 in order to encompass the main part of the unrest episode and the first days of the eruption. This allows us to identify and analyze the main gravity anomalies that occurred during the building up of the eruption. We describe here the methodology used and the data obtained, and then discuss them in terms of the magma movements occurring inside the upper lithosphere and in the volcanic edifice.

2. Background information on the geology of El Hierro and the 2011–2012 submarine eruption

El Hierro is the youngest and westernmost of the Canary Islands, a group of volcanic ocean islands located on the Atlantic side of the African plate, 150 km off the coast of Morocco (Figure 1). They originated as a result of an intra-plate magmatic episode lasting over 40 Ma [*Araña and Ortiz,* 1991] that gave rise to Holocene volcanism on all of these islands. El Hierro is a composite shield structure created by a combination of different volcanic edifices, which rises from 4000 m b.s.l to a maximum altitude of 1501 m a.s.l. and has a surface area of about 279 km^2 [*Guillou et al.,* 1996; *Carracedo et al.*, 2001]. The onshore geology of El Hierro shows three giant lateral collapses, namely Las Playas, El Julan and El Golfo (Figure 1), and the San Andrés fault (on the NE flank of the island) that could correspond to an aborted lateral collapse [*Day et al.*, 1997]. El Hierro has three well-defined ridges lying at 120º that concentrate all the Holocene volcanism, the most recent being the southern ridge that extends for about 40 km with a height of 2000 m above the sea floor

[*Münn et al.*, 2006]. Recent geodetic and gravimetric studies have investigated the crustal structure of El Hierro using gravity inversion [*Montesinos et al.*, 2006], as well as its elastic response to body-tide forces [*Arnoso et al.*, 2011]. Most recently, *Gorbatikov et al.* [2013] have studied the deep crustal structure of El Hierro using a micro-seismic sounding technique to create a 3D velocity model of the island's internal structure, which has revealed the existence of several local heterogeneities, as already noted by *Montesinos et al* [2006]. In fact, *Gorbatikov et al*. [2013] highlight the existence of a reservoir of solidified magma to a depth ranging between 15–25 km, located at the northwest of El Hierro, and connected with the formation of the younger part of the island. Other subsurface shallow structures identified as well by the density contrast model of *Montesinos et al.* [2006], seem associated to the southward migration of hypocenters along the contact surface of this reservoir and a high-velocity structure, which divides two large low-velocity bodies, one of them containing the solidified magma accumulation zone.

The 2011–2012 submarine eruption on El Hierro was preceded for nearly three months by an intense seismic swarm and important ground deformations, as reported by *López et al*. [2012] and *Ibáñez et al.* [2012]. These authors state that seismic unrest started on July 19, although dozens of local events had already been detected two days beforehand. More than 12000 localized earthquakes occurred up to the onset of the submarine eruption on October 10, the largest of which was of magnitude 4.3 M_{bLg} according to the earthquake catalogue of the Spanish Instituto Geográfico Nacional (IGN). Initially, the seismicity was of low magnitude (< 3.0 M_{bLg}) and two months after the beginning of the period of unrest, the earthquakes were still mostly focused on the north of the island at depths of 10–15 km (Figure 2a). In mid-September, seismicity began to migrate towards the south of the island and a slight increase of up to 17 km in the hypocentral depth was observed. In addition, both the magnitude of the earthquakes and the ground deformation rate increased during this period. By late September 2011, most of the earthquakes were located offshore to the southwest of the island, but with greater magnitudes. Early October, various episodes of deflation-inflation were noted by the GPS stations of the IGN network at different sites on the island. Variations in other geophysical parameters such as differences in magnetic observations at different stations and several peaks in ^{222}Rn concentration were also observed [*López et al.*, 2012]. Then, the hypocenters migrated southeastwards through the submarine flank of the southern ridge and a M_{bLg} 4.3 event occurred on October 8 at a depth of 12 km and 1.5 km from the coast (Figure 1). Only few shallow (1–4 km depth) earthquakes

followed this event (Figure 2b), suggesting that the magma approached the surface at the onset of the submarine eruption asseismically [*Martí et al.*, 2013]. The eruption started on October 10 at 04:15 UTC. At this point, a harmonic tremor signal appeared on the seismic records and continued for several weeks until the end of the eruption. The high-amplitude tremor signal overlapped the gravity records during the first days after the onset of the eruption. The eruption lasted for 4.5 months and constructed a new 220-m high volcanic edifice about 1 km in diameter at the base, which reaches 300 m b.s.l. at a distance of 1.8 km from the coast [*Rivera et al*., 2013].

3. Methodology and data acquisition

We acquired continuous gravity measurements from two different locations collected during different stages in the seismo-volcanic processes taking place between August 6, 2011 and October 15, 2011. The first observation site, LA (Figure 1), was located in the north of the island around El Golfo embayment in a private house in the village of Los Llanillos at 276 m a.s.l. The gravimeter was installed in the cellar on concrete base of 40 cm thick. The site was selected for its proximity to the seismic swarm that was located in this area at the beginning of the seismic process (Figure 1). A GPS antenna belonging to the IGN geodetical network [*López et al.*, 2012] was installed directly above the gravimeter on the house roof during the same observation period.

Due to the southwards migration of the seismic activity, the gravimeter was moved to a second site in the village of El Pinar at the end of September 2011. The site, Aula de la Naturaleza (AU) (Figure 1), is located near the geographic center of the island at 950.5 m a.s.l and 6.5 km SE from the site LA (Figure 1). The gravimeter was installed on a concrete pillar fixed to the bedrock at a depth of 30 cm inside a small room where it was protected from humidity and air currents. No GPS antenna was available at this site, although two relatively close permanent GPS stations belonging to the IGN network, HI01and HI08 (Figure 1), were installed 4 and 1 km away, respectively. In addition, a short base-length bi-axial tiltmeter (model Applied Geomechanics 701-2A) that records tilts in two orthogonal horizontal directions was positioned on a pillar next to the gravimeter from the end of September 2011 onwards [*Arnoso et al.*, 2012].

Previous tidal gravimetry studies had been conducted using a LaCoste & Romberg Graviton-EG spring gravimeter at site AU during 2008 [*Arnoso et al.*, 2011]. This provided us with a priori knowledge of the site's possibilities, as well as the stability and quality of the gravimetric measurements it could generate. Thus, we expected that the comparison of the

tidal observations with the theoretical body-tide models at this site could be carried out with an accuracy of 0.1%, as reported by *Arnoso et al.* [2011]. Details of the observations at sites LA and AU are summarized in Table 1.

The gravimeter used in this study was a Micro-g LaCoste's *gPhone,* an updated version of the classical LaCoste & Romberg (LCR) zero-length spring (model G) gravimeter, which has a double-oven thermal system that provides more precise temperature stability, a new beam-nulling system, a true vacuum seal that is completely insensitive to buoyancy changes due to atmospheric changes, and 0.1 μGal resolution in the frequency domain (see http://www.microglacoste.com/relativemeters.php). Many studies have confirmed the stability and accuracy of spring-type gravimeters when detecting gravity variations in active volcanic areas and the LaCoste&Romberg and Scintrex gravimeters are the most commonly used [*Brown et al.*, 1991; *Budetta and Carbone*, 1997; *Berrino et al*, 2000; *Carbone and Greco*, 2007]. In order to study the performances of the meter in terms of resolution, accuracy, noise level, and long-term stability the gPhone-054 used here was compared to the superconducting gravimeter SG-C026 at site J9 in Strasbourg (France) during 2008 [*Riccardi et al.*, 2011]. Conclusion achieved from this gravimetric comparison showed that the gravimeter behavior both in the tidal and seismic bands is satisfactory, even better than standard spring gravimeters (zero-length metal or quartz-type sensors). However, the instrumental drift rate is still greater than in a superconducting gravimeter and some uncertainties may be present in drift modeling when gravity fluctuations are small. Nevertheless, most uncertainties can be solved if meteorological perturbations can be modeled with enough accuracy and drift behavior is closely controlled or, as in the case of this study, long-term gravity variations are sufficiently large to be distinguished from other known and easily modeled effects.

It is well known that the time-variable gravity signal is composed of different contributing signals [*Torge*, 1989] including solid Earth tides, which add tens of μGal to the amplitude signal and can be easily modeled by different software packets depending on the final desired application [*Dierks and Neumeyer*, 2002]. Ocean tidal loading, atmospheric loading, and polar motion are other known factors that are included in the gravity signal. To achieve a residual gravity signal with the greatest geophysical significance, other parameters are usually sampled together with the gravity records. The core gravity sensor of the gPhone by design should be slightly influenced by environmental effects such as air pressure and temperature variations that in turn increase the non-linear drift problem, which is decisive for the purposes of volcano monitoring [*Budetta and Carbone*, 1997; *Berrino et al.* 2006, *Greco*

et al., 2012; *Crossley et al.*, 2013]. During this study, raw gravity data were sampled at 1 Hz frequency. Other parameters were also measured at different sampling rates: leveling instrument, atmospheric pressure, internal pressure sensor, air temperature, internal sensor temperature, humidity. Rainfall data indicated that no significant precipitation fell during the observation period and so the corresponding gravity effect was not evaluated.

Although the most important limitation of spring gravimeters is still the unpredictable drift behavior occurring during long-term observations, previous results gathered with a LCR gPhone-054 gravimeter operating at the J9 gravimetric observatory in Strasbourg (IPGS-EOST, France) confirmed suitable drift rates of a maximum of about 10 µGal/day and quick drift stabilization after installation. As well, no significant differences in its drift-rate evolution were observed over time [*Riccardi et al.*, 2011]. After its testing in Strasbourg, the gPhone-054 was moved to the atmospheric observatory of Izaña (Spanish AEMET) on the island of Tenerife (Canary Islands, Spain) for 1.5 years, where its stabilized drift-rate behavior was within the range of 0 to –2.0 µGal/day for the year before it was installed on El Hierro (Figure 3). This behavior fit in with the manufacturer´s guidelines, which indicate that after 1-2 years, the drift rate should fall substanlially (gMonitor User´s Manual, 2008). The instrumental drift changed drastically at sites LA and AU on El Hierro just before and during the period corresponding to the submarine volcanic eruption. After the eruption ended, the drift rate stabilized at an average value of about –1.0 ±0.5 µGal/day. To model the instrument drift from the signal showed in Figure 4, a linear fit was applied to the observed gravity data, after spikes and tilt-induced gravity effect were removed. Except for the first week after the installation of the gravimeter when the best fit corresponds to a second-degree polynomial (Figure 4c).

To attain the residual gravity signal, that is, the time gravity variation *free of perturbations,* several corrections were applied. Following a common procedure for processing time gravity series [*Hinderer et al.*, 2007; *Crossley et al.*, 2013], the residual gravity, g_{res}, can be expressed as

$$g_{res} = g_{obs} - g_m \tag{1}$$

where g_{obs} is the observed gravity data and g_m all known modeled signals. Thus, contributions from solid Earth and ocean tides, atmospheric pressure, meteorological effects (air temperature, humidity), polar motion and drift have to be subtracted from the recorded

gravity series.

The largest signal in the observed gravity data is produced by Earth tides. Tidal deformation of the Earth represents the elastic response of its body to gravitational accelerations produced by the Moon and the Sun and, to a lesser extent, other celestial bodies. The tidal forces can be described with high reliably and precision and, commonly, solid Earth and ocean tides are modeled with a high accuracy. Gravimeters measure tidal gravity variations at the Earth's surface with very high signal-to-noise ratio. Those variations, which occasionally may exceed 250 μGal, are a source of noise for many other geophysical measurements. The analysis of tidal gravimetric observations provides amplitude ratios and phase differences, in terms of the tidal waves that represent the response of the Earth's body to tidal forces, between observed amplitudes and phases and they respective theoretical calculations. Harmonic analysis methods are the most common approach used to model the tidal signal. Thus, a multiple regression model in the time domain is derived from a multiple input-single output system, through [*Neumeyer*, 2010, *Wenzel*, 1997]

$$y_t = \sum_{j=1}^{n} H_j A_j \cos(2\pi\omega_j t + \phi_j + \Delta\phi_j) + \sum_m R_{m_\omega} z_{m_\omega}(t) \quad (2)$$

where y_l represents the gravity observation at a time t, A_j, and ϕ_j are the amplitudes and phases of the tidal waves for frequencies ω_j (e.g. calculated from a tide generating potential), $z_m(t)$ is the additional signal included in the regression model (as for instance the air pressure). The amplitude factor H_j, the phase shift $\Delta\phi_j$ and the regression parameter R_m, are the unknowns estimated by least square fit of the observations. Here, we have used the software packages VAV [*Venedikov* et al., 2003] and ETERNA [*Wenzel*, 1996] that are widespread applied for tidal analysis purposes. Performance of both packages is similar when tidal parameters are estimated, although some differences exist in the filtering of the gravity data and in the treatment of statistics of the signal [*Dierks and Neumeyer*, 2002]. Thus, a previously calculated tidal model [*Arnoso et al.*, 2011] was used for testing tidal gravimetry results with the gPhone-54 at sites AU and LA and was then used to subtract body-tide and ocean-tide loading effects for computation of residual gravity.

Atmospheric pressure contribution to gravity signal is spread over a wide spectral domain and its magnitude can reach a value of about 30 μGal at certain locations. Atmospheric pressure effect is usually reduced from gravity signal estimating an empirical

transfer function (known as barometric admittance) between gravity and local air pressure changes. The 90% of the total pressure effect can be removed using the empirical approach and an approximate barometric admittance of about –0.3 μGal/hPa is commonly retrieved for continental stations, away from the coastlines [*Spratt*, 1982]. In our case, a local atmospheric correction was applied by adjusting the respective scalar coefficient for each observation site using the software VAV, which fits the gravity-pressure admittance together with the tidal parameters [*Venedikov et al.*, 2003]. The admittances were found to be –0.32 ±0.04 and –0.34 ±0.02 μGal/hPa for LA and AU, respectively. Those admittance factors are used to subtract the atmospheric pressure contribution from the raw gravity data when computing the residual gravity.

The gravity effect of the polar motion, the so-called pole-tide, is a consequence of the small movements of the Earth's rotation axis within the Earth. The gravity fluctuation, Δg_p, for a site at the Earth's surface can be computed using the time series of instantaneous pole coordinates ($x(t)$, $y(t)$) at time t, provided by the International Earth Rotation Service (IERS) with a resolution of 1 day, through [*Melchior*, 1993]

$$\Delta g_p = \delta_p \Omega^2 a(x(t)\cos\lambda + y(t) sin\lambda) sin2\phi \quad (3)$$

where a is the geocentric radius, (ϕ, λ) the geographic coordinates and Ω the mean rate of Earth's rotation Here $\delta_p = 1 + h - \frac{3}{2}k$ is the second degree gravimetric amplitude factor, in which h and k are the Love numbers for the body tides. The peak to peak amplitude of the gravity effect thus calculated for the observing period was about 3.2 μGal.

Instrumental effects related to meteorological perturbations such as those produced by rainfall and variations in air temperature and humidity were expected to be very low in the short observation periods, during which the gravity residuals underwent remarkable changes. Correlation between relative air humidity and temperature can be often significant and the gravimeter response depends on the different construction types and of their electrostatic feedback system [*El-Wahabi et al.*, 1997; 2000; *Palinkas*, 2006; *Hegewald et al.*, 2011]. Figure 4g show the residual gravity signal observed at LA and AU sites during the periods where remarkable changes were observed, together with the respective local air temperature variations. In none of the cases presented here, a correlation was found with these meteorological parameters. Air temperature variations at the observing sites, however,

influence the gravimeter levels. It is well known that instrument tilts can produce apparent gravity changes, which can lead to variations in instrumental drift behavior and therefore may mask other geophysical signatures related to volcanic activity [*Riccardi et al.*, 2009]. The tilt-induced gravity effect Δg when the gravimeter's axis of measurement is tilted an angle ϕ with respect to the vertical plumbline, is given by

$$\Delta g = (g_0 - g_0 cos\phi) \quad (4)$$

where g_0 is the local gravity. For small angles, expressing $cos\phi$ in terms of Taylor's series expansion, it can be followed [*Hinderer et al.*, 2007]

$$\Delta g \approx \frac{1}{2} g_0 \phi^2 \quad (5)$$

Assuming g_0 = 9.8 ms^{-2} and expressing ϕ in radians the dependency of gravity on tilt changes can be expressed as follows $\Delta g/\phi^2 = 4.9\ ms^{-2}/rad^2$. It means that if the gravimeter is tilted by 100 μrad will induce a reduction in gravity of 4.9 μGal.

Other significant contribution of the observed gravity signal come from the hydrology (water table, soil moisture, and rainfall). Thus, changes in water storages, soil moisture or groundwater can influence gravimetric observations by up to tens of μGal. Its determination becomes complex due to its variability, produced by water balance at observing sites, as well as to the length scales that makes necessary to investigate the soil moisture conditions in the vicinity of the gravimeter site [*Hinderer et al.*, 2007; *Harnisch and Harnisch*, 2006]. In our case, however, no effects of hydrology were corrected due to the absence of rivers and/or water reservoirs, together with the extremely dry conditions of the island during the observation period.

Following the procedure described above, the respective residual gravity was obtained at the observation sites LA and AU after modeling with some confidence all known signals. The effects produced by tilts, atmospheric pressure and polar motion were all calculated and reduced from observed gravity data. Solid Earth and ocean tides, as well as instrument drift, were modelled following the harmonic analysis method, and likewise were subtracted from the observed gravity. Then, the gravity signatures due to the studied seismo-volcanic unrest that preceded the El Hierro eruption could be studied by interpreting these remaining gravity residuals.

4. Observed anomalies

Remarkable gravity changes were found in the gravity residuals (i.e. after removing body and ocean tides and gravity changes induced by tilts and atmospheric pressure effects) during the different periods before the onset of the eruption at both sites LA and AU.

From the date of the installation of the gravimeter (6 August 2011) until September 15, few fluctuations were observed in the residual gravity signal (Figure 4g) of small amplitude (±2 μGal). During this period, seismicity was concentrated at the north of the island and at about 11 km in depth. The lack of a significant time correlation with other geophysical or geodetic changes hindered the identification and interpretation of those small anomalies in the gravity records.

On September 15 at 16:37 UTC a remarkable change in the trend of the residual gravity signal was recorded at site LA that ranged from 0 to −24 μGal/day (Figure 4g). From 11.40 UTC onwards on September 17 (i.e. 43 hours later) the trend was reduced to −1 μGal/day and the gravity signal decreased almost linearly for a total amount of about 45 μGal during those two days. The beginning of this anomaly coincided with a 100 μrad offset of the gravimeter's longitudinal level. However, no significant changes were observed in either the transversal level or the other instrumental data recorded at the same time. The vertical displacement of the GPS antenna installed at the same observation site increased by about 0.3 cm during same days (Figure 4e), which coincided with the general trend observed at other GPS stations on the island [see *López et al.*, 2012] following the inflation episode preceding the eruption. There was no evidence of any type of anthropogenic noise at the time, although we cannot discard this possibility. We checked the gravimeter's response to other similar tilt changes to rule out incorrect leveling. All experiences done showed us that the instrument drift suffered only noteworthy changes after power failures or transportation. Even in the worst testing case (that it, driving a shock on the gravimeter whilst operating), no changes in the instrument drift is observed. Moreover, instrument drift never exceeds 10 μGal/day during the observing periods up to date. Therefore, although the tilt of the longitudinal level could have a purely instrumental origin, the results of the test performed did not explain such large variations in the gravity residuals and so we assumed that phenomena related to seismo-volcanic activity were responsible for the gravity variations occurring during this period. In a similar context, tilt changes of tens of microradians ranging from hours to days were reported by *Bonaccorso and Gambino* [1997] during activity on the volcano Etna as a consequence of magma

displacements preceding and accompanying the beginning of the 1991–1993 eruption. Figure 5 shows an example of co-located measurements made at AU site by both levels of gPhone-054 and the bi-axial tiltmeter Applied Geomechanics 701-2A (AGI) installed there. After removing contributions from tides and diurnal temperature variations, only the X-axis of AGI exhibits a tilt offset of about −0.4 μrad during the occurrence of the M_{bLg}4.3 earthquake of October 8, 2011 [*Arnoso et al.*, 2012]. Similarly, the longitudinal level displays an offset of −0.7 μrad, which is coherent with tiltmeter signal, and thus indicating the capability of the gravimeter levels to detect real tilt changes. Therefore, the effect of a ground deformation of volcanic origin could be present on the tilt recorded by the longitudinal level of gPhone-054 during September 15 at LA site. Unfortunately, no other tiltmeters that could have confirmed these fast ground deformations were installed on El Hierro during this period. However, although the seismic activity showed no increase in the magnitude, number of events, or any substantial variation in the depth of the epicenters, a clear southward migration (Figure 2a) did take place from the second half of September onwards, as was confirmed recently by *Dominguez et al.* [2014].

Possible earthquake-induced gravity changes from continuous observations at site AU were observed during the seismic swarm stage on October 7 and 8, 2011. The magnitudes of the seismic events of the whole unrest episode peaked and the IGN network recorded a sequence of earthquakes with magnitudes exceeding M_{bLg} 3.6 (Figure 1). Two step-like gravity increase (positive step) of 2.5 μGal are clearly visible on the residual gravity signal during those days (Figure 5a).By contrast, the positive step of October 8th coincided in time with the event of magnitude M_{bLg} 4.3 recorded by the IGN seismic network whose epicenter was located at a depth of 12 km about 8 km from site AU and could be interpreted in terms of co-seismic gravity changes.

A new anomaly detected on the residual gravity coincided with the start of the volcanic tremor, assumed to correspond to the onset of the eruption [*Martí et al.*, 2013]. Figure 6a shows the gravity signal observed at site AU during the first days of the eruption, from October 8–15, 2011. The effect of the volcanic tremor is clearly visible on the gravity record from October 10 onwards and induced a high level of background noise. To study the gravity signal, we calculated the respective residual gravity and then filtered it using a cut-off frequency of 24 cpd (cycles per day) and a window length of 480 data points. This enabled us to observe a clear change in the trend of the residual gravity, from 0 to −25 μGal/day since the onset of the tremor on October 10, even though the gravimeter's levels were running

without significant variation despite being highly influenced at high frequencies by the volcanic tremor. This trend continued for just one day, until October 11 at 05:00 (UTC). Then, the trend of the residual gravity curve changed drastically, that is, episodic gravity changes varying from 10 to –90 μGal were observed over the next two days (see Figure 6), during which time neither substantial ground tilts nor height change (as measured by GPS network Spanish IGN) were observed at site AU (see Figures 4b and 4e, respectively).

Finally, in addition to the anomalies described above it is also worth mentioning the anomalies detected in the high-frequency band of the gravity signal. In the spectrum computed from the original 1-Hz record of the gPhone-054 in the five days prior to the onset of the tremor (up to October 10), the amplitude of the observed gravity signal at frequencies between 0.05–0.4 Hz, known as the microseismic band [*Longuet-Higgins*, 1950], increased up to 2.5 times (see Figure 7). On October 6–8 and until the occurrence of the M_{bLg} 4.3 earthquake, the amplitudes corresponding to the frequencies between 0.25 and 0.40 Hz reached the highest value. Usually, perturbations in this frequency band are due to meteorological effects. From a few hours before the M_{bLg} 4.3 event and up to the beginning of the volcanic tremor on October 10, a well-defined frequency signal appeared that was located around a narrow band centered on 0.2 Hz, and which became more evident on October 9 (Figure 7-right). This well-defined signal is known as the secondary peak of the microseismic band and it does not appear often at the gravity records. Meteorological conditions during this period were stable and air pressure, temperature, humidity and wind speed do not show any significant variation (Spanish Meteorological Agency, http:// www.aemet.es).

5. Modeling time gravity variations

- September 15th to 17th, 2011: 45μGal gravity decrease.

We want to explain the observed anomaly on the residual gravity found at site LA during September 15–17. We assume that it is due to magma migration following the seismological interpretation by [*Martí et al.*, 2013]. As we mentioned above, vertical displacement measured by the GPS on September 15–17 was negligible at LA, that is, the free air gradient effect corresponding to 0.3 cm of vertical displacement is not enough to explain the gravity decrease of 45 μGal (an elevation change of about 15 cm would be required). Also, *González et al.* [2013] used Interferometric Synthetic Aperture Radar (InSAR) technique to model ground deformation to constrain the dynamics associated with the magmatic activity during the pre-eruptive and coeruptive phases of the 2011-2012 El

Hierro submarine eruption. Their result does not assess any clear ground deformation around LA site for the days 15–17 of September. Moreover, the interferograms calculated by those authors do not exhibit a deformation pattern at LA during the complete period of southward seismic migration (mid-September to early October). Therefore, the lack of vertical ground deformation makes difficult to explain the gravity decrease recorded at this observing site. However, it is more likely that both a mass loss (Bouguer effect) related to magma drainage and a density decrease due to the fracturing could produce such gravity variation. Accordingly, we provide the respective models based on mass loss and density decrease process. On the one hand, we modelled the gravity decrease assuming a mass loss due to the magma migration through dikes. The associated gravity effect can be approximately calculated as if produced by a 2-D vertical sheet [*Nettleton*, 1976]

$$\Delta g = 2G\Delta\rho w \ln\left[\frac{(h+z)^2 + d^2}{h^2 + d^2}\right] \tag{6}$$

where G is the Universal Gravitational Constant (6.6742×10^{-11} $m^3kg^{-1}s^{-2}$) and $\Delta\rho$ the density change; w and h are, respectively, the thickness and the vertical length of the sheet; z is the depth of the upper part of the sheet and d the horizontal distance (Figure 8). We have considered a dike of 5000 m of vertical length and 10 m thick, at a distance to the gravimeter site LA based on the seismicity occurred prior to September 15th. The values for the gravity effect thus calculated, placing the dike at different depths and depending on the density contrast are shown in Figure 9c. Thus, for instance, if we select a density contrast of –250 kg/m^3 the gravity variation found at 12 km depth is of about –25 μGal. The model establishes several possibilities to achieve a gravity value based on the selected density contrast and for the depths ranging between 10 to 12 km.

On the second hand, we want to model the gravity variation due to density decrease. Thus, we take into account the available data from the IGN seismic catalogue up to September 15, 2011, and consider the fact that 90% of the events ($M_{bLg} > 1$) were located between latitudes 27°.7211N–27°.7819 N. Then, we approached the seismicity path as follows: i) The distance between these coordinates was divided by bands spaced every 50 m, from north to south, so that the minimum width of the band contained enough events to perform a reasonable statistical analysis; ii) the mean value and the standard deviation within each band were calculated for the respective hypocenters contained therein; iii) these mean

values were fitted to a straight line with an azimuth of 149º E located at a depth of 11 km; and, finally, iv) the volume occupied by seismic events was defined with prisms spaced every 50 m, from north to south, centered on the previously calculated line (point iii), with sides bounded by the mean value of the standard deviation in each direction (Figure 9a)

a). Now, we supposed that mass migrating southward through dikes or sills to a deeper level would have produced changes in the gravity as magmatic material filled the different density contrasts of the medium. Therefore, it is reasonable to assume that part of the gravity variation recorded during September 15 to 17 was a consequence of a density decrease (redistribution of mass) provoked by a geophysical process along the fractured zone that was limited by the modeled volume occupied by the seismic events (point iv). To explain this behavior, the theoretical gravity variation due to a decrease in the density of the subsurface masses was calculated. By taking into account different subsurface models, the density of the prismatic structures defined previously (point iv) was substituted by a new density. Then, the *Nagy* [1969] formulation taking into account both the old and new density values was applied to calculate the gravity attraction at site LA. This approach was applied in two different cases (Figure 9d): a) The first case was based on the previous subsurface density model used by *Montesinos et al.* [2006], which was obtained by gravimetric inversion techniques. Former density values for each prism were taken from this model and then replaced by new ones; b) in the second case, we used a simpler model assuming that the previous density was the same for each prism and a mean density value of 2510 kg/m^3 was adopted for the whole subsurface of the island [*Montesinos et al.*, 2006]. Consequently, considering the previous gravity change modeled by the mass loss effect, a variation of density between 2400 to 2510 kg/m^3 due to the fracturing would produce a gravity decrease of about 0 to 20 μGal (see Figure 9d), which should be considered to attain the observed gravity variation of –45 μGal.

In both of the above cases, the density of the defined fractured area decreased (Figure 9d). This fact is consistent with the migration of magma into a deeper area in the south of the island. Bearing in mind that long-term drift in the gPhone-054 is small [*Riccardi et al.* 2011], and that part of the modeled linear drift could correspond to seismo-volcanic process, the impact on the residual gravity is minimal and about 10 μGal. This difference is not enough to vary our reasoning, that is, that the southwards migration of seismicity and the subsequent redistribution of subsurface mass caused a density decrease. This fact, and the gravity decrease produced by mass loss due to magma migration were both the most probable causes of the diminishing residual gravity signal.

- *October 7th to 8th, 2011: co-seismic gravity changes*

The gravity change we observed on October 8, 2011, coincided in time (20:34h UTC) with the most important seismic event during the whole episode of unrest, which has been interpreted as the moment two days later that a path for the magma to the surface was opened and provoked the submarine eruption [*López et al.*, 2012; *Perez-Torrado et al.*, 2012; *Martí et al.*, 2013]. Other gravity change of similar amplitude, and coinciding with the occurrence of various seismic events of magnitude M_{bLg} > 3.6 recorded 20 hours before (Figure 5a), could be likewise related with the rupture process and magma ascent to the surface. Approach of these co-seismic gravity changes is feasible through calculation of the responses of a multi-layered viscoelastic-gravitational half-space to point dislocation sources [e.g., *Wang et al.*, 2006]. However, gaps in coverage of the IGN seismic network due to size and geometry of El Hierro Island increase the uncertainty in the model of the focal mechanism. Furthermore, a recent study by *Dominguez Cerdeña et al.* [2014] that considerably improves the previous hypocentral location of the seismic swarm preceding the submarine eruption, provide errors of 4.7 ±2.1 km in a horizontal sense and 4.3 ±1.8 km in depth, with 90% confidence. Then, seismic moment tensor solution for the M_{bLg} 4.3 earthquake does not allow an accurate definition of the rupture length that matches the focal mechanism. This fact introduces large uncertainties in the theoretical calculation and prevent us to obtain a reasonable calculation of the co-seismic gravity effect.

- *October 10th to 13th, 2011: gravity variations during the eruption onset*

The eruption started at 04:15 (UTC) on October 10, 2011, when a harmonic tremor signal showed up in the seismic records of the IGN stations [*López et al.*, 2012]. The seismicity prior to the tremor signal indicates that the initial eruptive vent was probably located about 5 km offshore, on the submarine flank of the island's southern ridge (see Figure 1). However, no eruptive proof (i.e. fragments of lava bombs) or any other observational evidence pertaining to these initial stages of the eruption were observed on the surface until two days later. *Martí et al.* [2013] pointed to the magma ascended through a dike on the southern ridge and that during the first three days of the eruption the eruptive focus migrated northwards for about 3 km along the eruptive fissure until it intersected a NE-SW regional normal fault; from this moment on, a central conduit was generated and the construction of a cone began.

Taking into account the fact that no significant variations in height were observed and

that the gravimeter leveling seemed only to be altered by the high frequencies caused by the tremor, most of the gravity anomaly detected on October 10–13 can be linked to subsurface redistributions of mass. Similar anomalies in the gravity signal were reported, for instance, by *Branca et al.* [2003] and *Carbone et al.* [2007] when describing a short-lived explosive event that marked the onset of the 2002 eruption on Etna. In that case, the observed gravity decrease (about -400 μGal) was interpreted as a magmatic intrusion occurring after the development of a fracture system located about 1 km from the gravity station. In our case, assuming that the M_{bLg} 4.3 earthquake on October 8 opened a fracture, the gravity changes observed on October 10–12 at site AU (about 10–12 km from the volcano) would be related to changes in subsurface mass provoked by the opening of the eruptive fracture and by the movement of magma along it. Using the equation (6), we approximately calculated the associated gravity effect as if produced by a 2-D vertical sheet. Based on the previous density-contrasts model obtained by *Montesinos et al.*, [2006], the host rock density was taken to be 2510 kg/m^3. Thus, the gravity variation that reached site AU was computed for a variable distance (*d*) from the source, assuming a vertical length of 5000 m according to the model of density contrasts around the location of the volcanic eruption (Figure 10). There, the interface between different low- and high-density structures close to the new volcano edifice indicated a clear northwest-southeast alignment, coinciding with the fracture indicated by *Martí et al.* [2013]. Such structures in the density contrasts are not preserved below a depth of 6000 m (see Figure 5 in *Montesinos et al.*, 2006) and so the dike cannot be modeled with such precision at any further depth.

Our results for the gravity effect thus calculated are given as a function of the distance between the gravimeter site and the vertical sheet (i.e. an approximation of a dike) and for varying thicknesses of 3–10 m (Figure 11). The gravity values for the distances 9500–12000 m from the gravimeter site assuming a 5–7-m-thick dike are about –80 to –40 μGal. They are consistent with the observed gravity variations (Figure 6a), the change in the distance being justified by the northward migration of the eruptive focus (i.e. towards site AU) by about 3 km during the first days of the eruption, as described by *Martí el al.* [2013].

Looking in detail at Figure 6a, it can be seen that on October 11–13, 2011, the residual gravity variations fluctuated considerably and reached –90 μGal at noon on October 11 and at the beginning of October 12. Superimposed on the residual gravity curve, Figure 6b shows the body tide vertical strain calculated for site AU for the same time period. An apparent correlation between the two curves can be seen for the diurnal frequencies. We propose that the residual gravity variations recorded at site AU during the first three days of

the eruption might have been influenced by tidal strain. At that moment, a displacement along the eruptive fissure could have occurred, followed by a compression of different parts of the plumbing system due to its progressive decompression and magma withdrawal. This fact is coherent with and could explain the gravity variation observed at site AU during the initial stages of the eruption, in which periodic tidal strain could have played an important role. However, the quantification of the potential role of the periodic tidal strain in the triggering of the eruption would require a more precise analysis that is beyond the purpose of this study.

- High-frequency gravity signal of October 6th to 11th, 2011.

According to *Longuet-Higgins* [1950], the frequency band 0.1–0.3 Hz corresponds to the secondary microseismic peak. The spatial origin of this peak seems to be due to both coastal and deep-ocean sources [*Cessaro,* 1994; *Chevrot et al*., 2007] and the amplitude of the signal can be correlated with sources of different origin such as bathymetry, ocean-wave height, wind, storms, and hurricanes [e.g. *Kedar et al.*, 2008]. Regardless of the origin, the final effects are pressure pulses at sea, which propagate to the sea floor and then generate microseismicity. In our case, as mentioned above, the M_{bLg}4.3 earthquake on October 8 probably opened the fissure that the magma used to ascend to the surface. The dramatic descent of the number of seismic events during the next two days (Figure 2b) also gives credibility to this assertion. Moreover, the magma ascended in an aseismic way with a velocity of 0.13 ms^{-1} on these days [*Martí et al.,* 2013]. Thus, a pressure overload on the seabed and the magmatic intrusion could have generated pressure pulses, which could have been the source of the observed high-frequency signal in the gravity records recorded before the onset of the eruption. This high-frequency signal found in the gravity records during the days before the submarine volcanic eruption at El Hierro suggests that these pressure pulses were probably not caused by atmospheric/oceanic effects but, rather, by the interaction of magmatic activity and the ocean. Similar cases have been described since the 1930s from the volcano Aso [e.g. *Sassa*, 1935; *Kubotera*, 1974; *Kawakatsu. et al*., 2000; *Zeng et al*., 2011]. However, more data (e.g. seismic, atmospheric pressure, tide gauges) still need to be analyzed if we want to fully understand the nature of the source of this signal and thus be able to connect it with a possible precursory signal.

6. Discussion

Gravity variations recorded by the gPhone-054 on El Hierro have provided an

interesting map of the time evolution of the gravity field during the various phases of the unrest episode that preceded the submarine eruption in 2011–2012.

Up to September 15, 2011, only small variations in the residual gravity had been observed, most generated by seismic swarms that coincided with the main phase of magma accumulation at the base of the oceanic crust (12–15 km b.s.l.) in the north of the island [*Martí et al*., 2013]. However, from September 15–17 onwards, a significant gravity decrease was observed at site LA (Figure 4g), coinciding with the initiation of the southward migration of seismicity and a slight increase in depth of the hypocentral location. In principle, this gravity change could be due to either (i) the redistribution of mass at depth caused by magma migration, (ii) variation in density, or (iii) a large variation in the height at the observation site. A combination of these three increases the number of possible sources of the gravity changes and so joint interpretation with other geodetic/geophysical data is necessary. One likely solution discussed above implies delimiting the disturbed area (the fractured zone) by locating the hypocenters and decreasing the host rock density value there (Figure 9d). Under these conditions, different processes could cause a change in the density. However, southward seismic migration to deeper crustal levels (after this period) is consistent with magma transport or drainage away from the gravimetric site occurred. Thereafter, gravity variation continued decreasing in magnitude, albeit at a lower rate, probably due to the remoteness of the seismicity.

On October 7–8, 2011, the gravimeter's levels underwent a series of rapid displacements linked to a seismic swarm characterized by several $M_{bLg} > 3$ events. Two increments of about 3 μGal in the amplitude of the residual gravity were recorded at site AU (Figure 5a), within a time interval of 20 hours. Although co-seismic gravity effect was not evaluated, the magnitude of those gravity changes coinciding with the M_{bLg} 4,3 event seems connected with the beginning of the rupture process regarding the magma ascent to the surface. From October 8 01:00 UTC onwards, lower magnitude events continued at the same location and no significant gravity variation was recorded. During this period, most of these events were concentrated in a narrow area to the south of the island. It is likely that the magma found a stress barrier here and began to generate differential stresses in its search for another path. It seems plausible that this path was provided by the effect of the M_{bLg} 4.3 event on October 8 at 20:34 UTC. In the previous section, the co-seismic gravity change associated with that event (about 2.4 μGal) was explained according to a tectonic process connected to the opening of the fracture, which allowed magma to reach the surface. Furthermore, during

the next two days shallower seismic events were recorded by the IGN stations, which indicates that the magma was rising. Likewise, a clear 0.2 Hz peak was identified in the high-frequency gravity signal (Figure 7), also recorded by the gPhone-054 at site AU. This frequency is usually associated with the secondary microseismic peak [*Longuet-Higgins*, 1950] and can be attributed to atmospheric perturbations. In this case, however, and in accordance with *Martí et al.* [2013], this signal should be interpreted as due to overpressure pulses generated by the magma when ascending to the surface prior to the onset of the eruption. The beginning of the submarine eruption was recorded by the gPhone-054 at site AU since the volcanic tremor was superimposed on the gravity signal (Figure 6a) from October 10 onwards. Firstly, a change in the trend of the residual gravity was clearly seen, decreasing at a rate of 25 μGal/day until October 11. We correlated this gravity anomaly with a main degassing phase throughout the fractured upper crust as the magma approached the surface and thus generated a density decrease and the tremor. Secondly, from October 11 at 04:41 UTC to October 12, the residual gravity signal reflected a change in the volcanic process, which was apparently correlated with tidal strain forces (Figure 6b). It is feasible that the tidal vertical strain partially drove the process until the final outflow conduit (i.e. the eruptive fissure) was completely open. During this time, the magnitude of the gravity decrease can be modeled as a 5–7-m-thick and 5-km-long dike intrusion varying in distance from the gravimeter depending on the northward migration of the eruptive focus (about 3 km) during the first days of the eruption [*Martí el al.*, 2013]. Although no significant changes were observed in the respective tilt excursion, the noisy response in the gravimeter's levels was due to the tremor. A closer look at Figure 6a reveals a rapid stabilization of the gravity signal from noon onwards on October 12, followed by a small upward jump of about 30 μGal, most probably caused by the complete opening of the outflow conduit. This fact could have reduced the pressure of the internal conduit and, consequently, caused the tremor to decrease in amplitude.

7. Conclusions

The potential of continuous gravity measurements carried out in active volcanic areas has been shown by the case of the 2011–2012 El Hierro (Canary Islands) submarine eruption. The recorded continuous gravity variations provide reliable data for modeling subsurface density changes, as well as magma movements during volcanic unrest. In this case, and in combination with other geodetic/geophysical techniques, a LaCoste & Romberg gPhone-054 spring gravimeter was used to monitor the activity during the unrest episode that started on

July 17, 2011. Various episodes of magma accumulation and migration occurring several kilometers from the observation sites were accompanied by significant gravity variations that we analyzed in four different stages: (i) magma accumulation in the north of the island, (ii) southward magma migration, (iii) magma ascent to the surface, and (iv) the eruption onset and the northward migration of the eruptive focus. Therefore, the recorded gravity variations are coherent with the causes of the unrest episode and can be understood as clear precursors of the submarine eruption that finally started on October 10, 2011 on the southern ridge of El Hierro. Additionally, the observations during the first days of the eruption, which exhibited an apparent correlation with body tide vertical strain, are consistent with the opening of the active fissure and the northwards migration of the eruptive focus.

Acknowledgements

Projects CGL2011-25494 and CGL2011-16144-E of the Spanish Ministry of Economy and Competitiveness and European Commission VULMAC-MAC/2.3/A7 (INTERREG) and VUELCO (FT7 Theme: ENV.2011.1.3.3-1; Grant 282759) partially supported this research. The authors are grateful to all colleagues from the Spanish IGN for their assistance in the maintenance of the LCR gPhone-054 during the observation period. We are also greatly indebted to every resident and to Cabildo Insular of El Hierro for helping with our research activities at site AU. The English text was revised and corrected by Michael Lockwood. Authors greatly acknowledge the comments given by Dr. L. Chardot and an anonymous reviewer that improved substantially the manuscript.

REFERENCES

Araña, V., and R. Ortiz (1991), The Canary Islands: Tectonics, Magmatism and Geodynamic Framework. In: A.B. Kampunzu and R.T. Lubala (Editors), Magmatism in Extensional Structural Settings. The Phanerozoic African Plate. Springer-Verlag, Germany, pp. 209-249.

Arnoso, J., J Fernández, R. Vieira, E. J. Vélez, A. P. Venedikov, (2000). Results of tidal gravity observations in Tenerife, Canary Islands. *Bulletin d'Information des Marees Terrestres, 132*, 10283–10290.

Arnoso J., J. Fernández and R. Vieira (2001), Interpretation of tidal gravity anomalies in Lanzarote, Canary Islands, *J. Geodyn., 31* (4), 341-354, doi: 10.1016/S0264-3707(01)00003-5.

Arnoso, J., M. Benavent, M. S. Bos, F. G. Montesinos and R. Vieira (2011), Verifying the body tide at the Canary Islands using tidal gravimetry observations, *J. Geodyn., 51* (5), 358-365, doi: 10.1016/j.jog.2010.10.004.

Arnoso, J., F. G. Montesinos, M. Benavent, E. J. Vélez (2012), The 2011 volcanic crisis at El Hierro (Canary Islands): monitoring ground deformation through tiltmeter and gravimetric observations, *Geophys. Res. Abst., 14*, EGU2012-5373.

Berrino, G. (2000), Combined gravimetry in the observation of volcanic processes in Southern Italy, *J. Geodyn., 30* (3), 371-388, doi: 10.1016/S0264-3707(99)00072-1.

Berrino, G., G. Corrado, and U. Riccardi (2006), On the capability of recording gravity stations to detect signal coming from volcanic activity: the case of Mt. Vesuvius, J. *Volcanol. Geotherm. Res., 150* (1-3), 270-282, doi: 10.1016/j.jvolgeores.2005.07.015.

Bonaccorso, A. and S. Gambino (1997), Impulsive tilt variations at Mount Etna Volcano (1990-93), *Tectonophysics, 270* (1-2), 115-125, doi: 10.1016/S0040-1951(96)00172-2.

Bonafede, M. and C. Ferrari (2009), Analytical models of deformation and residual gravity changes due to a Mogi source in viscoelastic medium, *Tectonophysics, 471* (1-2), 4-13, doi: 10.1016/j.tecto.2008.10.006.

Bonvalot, S., M. Diament and G. Gabalda (1998), Continuous gravity recording with Scintrex CG-3M meters: a promising tool for monitoring active zones, *Geophys. J. Int., 135* (2), 470-494, doi: 10.1046/j.1365-246X.1998.00653.x.

Branca, S., D. Carbone and F. Greco (2003), Intrusive mechanism of the 2002 NE-Rift eruption at Mt. Etna Italy inferred through continuous microgravity data and volcanological evidences, *Geophys. Res. Lett., 30* (20), 2077, doi: 10.1029/2003GL018250.

Brown, G.C. and H. Rymer (1991), Microgravity monitoring at active volcanoes: A review of theory and practice *Cahier du Centre Européen de Géodynamique et de Séismologie, 4*, 279-304.

Budetta, G. and D. Carbone (1997), Potential Application of the Scintrex CG-3M gravimeter for monitoring volcanic activity: results of field trials at St. Etna, Sicily, *J. Volcanol. Geotherm. Res., 76* (3-4), 199-214, doi: 10.1016/S0377-0273(96)00080-7.

Carbone, D. and F. Greco (2007), Review of microgravity observations at Mt. Etna: a powerful tool to monitor and study active volcanoes, *Pure Appl. Geophys., 164*, 769-790, doi: 10.1007/s00024-007-0194-7.

Carracedo, J. C., E. R. Badiola, H. Guillou, J. de la Nuez and F. J. Perez-Torrado (2001), Geology and volcanology of La Palma and El Hierro, Western Canaries, *Estud. Geol.,*

57, 175-273.

Cessaro, R. K. (1994), Sources of primary and secondary microseisms, *Bull. Seism. Soc. Am., 84* (1), 142-148.

Chevrot, S., M. Sylvander, S. Benahmed, C. Posolles, J. M. Levèvre, and D. Paradis (2007), Source locations of secondary microseisms in western Europe: Evidence for both coastal and pelagic sources, *J. Geophys. Res., 112*, B11301, doi: 10.1029/2007JB005059.

Crescentini, L. and A. Amoruso (2007), Effects of crustal layering on the inversion of deformation and gravity data in volcanic areas: An application to the Campi Flegrei caldera, Italy, *Geophys. Res. Lett., 34*, L09309, doi: 10.1029/2007GL029919.

Crossley, D., J. Hinderer, and U.Riccardi (2013), The measurement of surface gravity, *Rep. Prog. Phys., 76*, 046101, doi: 10.1088/0034-4885/76/4/046101.

Day, S.J., J.C. Carracedo and H. Guillou (1997), Age and geometry of an aborted rift flank collapse: the San Andres fault system, *Geol. Mag., 134* (4), 523-537, doi: 10.1017/S0016756897007243.

Dierks, O. and J. Neumeyer (2002), Comparison of Earth tides analysis programs, Bull. Inform. Marées Terrestres, 135, 10669-10688.

Domínguez Cerdeña, I., del Fresno, C. and Gomis Moreno, A. (2014). Seismicity patterns prior to the 2011 El Hierro eruption. *Bulletin of the Seismological Society of America, 104*, 567-575; doi:10.1785/0120130200

El Wahabi, A., H. J. Dittfeld and Z. Simon (2000), Meteorological influence on tidal gravimeters, *Bull. Inform. Marees Terrestres, 133*, 10403-10414.

El Wahabi, A., B. Ducarme, M. Van Ruymbeke, N. d'Oreyè and A. Somerhausen (1997),

Continuous gravity observations at Mount Etna Sicily and correlations between temperature and gravimetric records, *Cahiers du Centre Europeen de Geodynamique et de Seismologie, 14*, 105-119.

Furuya, M., S. Okubo, W. Sun, Y. Tanaka, J. Oikawa, H. Watanabe and T. Maekawa (2003), Spatio-temporal gravity changes at Miyakejima Volcano, Japan: Caldera collapse, explosive eruptions and magma movement, *J. Geophys. Res., 108*, B42219, doi: 10.1029/2002JB001989.

gMonitor User's Manual (2008). gMonitor Gravity Data Acquisition and Processing Software.

González, P. J., S. V. Samsonov, S. Pepe, K. F. Tiampo, P. Tizzani, F. Casu, J. Fernández, A. G. Camacho, and E. Sansosti (2013), Magma storage and migration associated with the 2011–2012 El Hierro eruption: Implications for crustal magmatic systems at oceanic island volcanoes, *J. Geophys. Res. Solid Earth, 118*, 4361–4377, doi:10.1002/jgrb.50289

Gorbatikov, A. V., F. G. Montesinos, J. Arnoso, M. Yu Stepanova, M. Benavent and A. A. Tsukanov (2013), New Features in the subsurface structure model of El Hierro Island (Canaries) from low-frequency microseismic sounding: an insight into the 2011 seismo-volcanic crisis, *Surveys in Geophysics, 34* (4), 463-489, doi: 10.1007/s10712-013-9240-4.

Gottsmann, J., L. Wooller, J. Martí, J. Fernández, A. G. Camacho, P. J. Gonzalez, A. Garcia, and H. Rymer (2006), New evidence for the reawakening of Teide volcano, *Geophys. Res. Lett., 33*, L20311, doi: 10.1029/2006GL027523.

Greco, F., C. Carmisciano, C. Del Negro, I. Loretti, A. Sicali, P. Stefanelli (2008), Seismic-induced accelerations detected by two coupled gravity meters in continuous recording

with a high sample rate at Etna volcano, *Annals of Geophysics*, 51 (1), 87-103, doi: 10.4401/ag-4441.

Greco, F., G. Currenti, G. D'Agostino, A. Germak, R. Napoli, A. Pistorio and C. Del Negro (2012), Combining relative and absolute gravity measurements to enhance volcano monitoring, *Bull. Volcanol., 74* (7), 1745-1756, doi: 10.1007/s00445-012-0630-0.

Guillou H., J. C. Carracedo, F. Perez-Torrado and E. Rodríguez Badiola (1996), K-Ar ages and magnetic stratigraphy of a hotspot induced, fast-grown oceanic island: El Hierro, Canary Islands, *J. Volcanol. Geotherm. Res., 73* (1-2), 141-155, doi: 10.1016/0377-0273(96)00021-2.

Harnisch, G. and Harnisch, M. (2006), Hydrological influences in long gravimetric data series, *Journal of Geodynamics, 41*(1-3), 276-287.

Hegewald, A., G. Jentzsch and T. Jahr (2011), Influence of temperature variations on the noise level of the data of the LaCoste and Romberg Earth tide gravity meter ET18, *Geochem. Geophys. Geosyst., 12*, Q04005, doi: 10.1029/2010GC003432.

Hinderer J., Crossley D. and Warburton R. J. (2007) Superconducting gravimetry Treatise on Geophysics vol 3 (Geodesy) ed T Herring, Gen. ed G Schubert (Amsterdam: Elsevier) pp 65–122.

Ibáñez J. M., S. De Angelis, A. Díaz-Moreno, P. Hernández, G. Alguacil, A. Posadas and N. Pérez (2012), Insights into the 2011–2012 submarine eruption off the coast of El Hierro (Canary Islands, Spain) from statistical analyses of earthquake activity, *Geophys. J. Int., 191*, 659-670, doi: 10.1111/j.1365-246X.2012.05629.x.

Kawakatsu H., S. Kaneshima, H. Matsubayashi, T. Ohminato, Y. Sudo, T. Tsutsui, K. Uhira, H. Yamasato and D. Legrand (2000), Aso94: Aso seismic observation with broadband

instruments, *J. Volcanol. Geotherm. Res., 101* (1-2), 129-154, doi: 10.1016/S0377-0273(00)00166-9.

Kedar, S., M. Longuet-Higgins, F. Webb, N. Graham, R. Clayton and C. Jones (2008), The origin of deep ocean microseisms in the North Atlantic Ocean, *Proc. R. Soc. London, Ser. A, 464* (2091), 777-793, doi: 10.1098/rspa.2007.0277.

Kubotera, A. (1974). Volcanic tremors at Aso volcano, In: L. Civetta, G. Gasparini, G. Luongo and A. Rapolla, Physical volcanology, Elsevier, Amsterdam, pp 29-48.

Longuet-Higgins, M. S. (1950), A theory of the origin of microseisms, Phil. Trans. R. Soc. A., 243, 1-35, doi: 10.1098/rsta.1950.0012.

López, C., M. J. Blanco, R. Abella, B. Brenes, V. M. Cabrera, B. Casas, I. Domínguez, A. Felpeto, M. Fernández de Villalta, C. del Fresno, O. García, M. J. García-Arias, L. García-Cañada, A. Gomis, E. González-Alonso, J. Guzmán, I. Iribarren, R. López, N. Luengo, S. Meletlidis, M. Moreno, D. Moure, J. Pereda, C. Rodero, E. Romero, S. Sainz-Maza, M. A. Sentre, P. A. Torres, P. Trigo and V. Villasante (2012), Monitoring the volcanic unrest of El Hierro (Canary Islands) before the onset of the 2011–2012 submarine eruption, *Geophys. Res. Lett., 39* (13), L13303, doi: 10.1029/2012GL051846.

Martí, J., V. Pinel, C. López, A. Geyer, R. Abella, M. Tárraga, M. J. Blanco, A. Castro and C. Rodriguez (2012), Causes and mechanisms of El Hierro submarine eruption (2011-2012) (Canary Islands*), J. Geophys. Res., 118* (3), 823-839, doi: 10.1002/jgrb.50087.

Melchior, P., (1983). The Tides of the Planet Earth, second ed. Pergamon Press, Oxford, 641 pp.

Montesinos F. G., J. Arnoso, M. Benavent and R. Vieira (2006), The crustal structure of El Hierro (Canary Islands) from 3-D gravity inversion, *J. Volcanol. Geotherm. Res., 150* (1-

3), 283-299, doi: 10.1016/j.jvolgeores.2005.07.018.

Münn S., Walter T.R. and Klügel A. (2006), Gravitational spreading controls rift zones and flank instability on El Hierro, Canary Islands, *Geol. Mag., 143* (3), 257-268, doi: 10.1017/S0016756806002019 .

Nagy, D. (1969), The gravitational attraction of a right rectangular prism, *Geophysics, 31* (2), 362-371, doi: 10.1190/1.1439779.

Nettleton, LL. (1976). Gravity and magnetics in oil prospecting. McGraw-Hill (New York), 464p.

Neumeyer, J. (2010). Superconducting gravimetry. In G. Xu (ed.), Sciences of Geodesy –I, Springer-Verlag, pp 339-413, doi 10.1007/978-3-642-11741-1_10

Pálinkás, V. (2006). Precise tidal measurements by spring gravimeters at the Station Pecný. *J. Geodyn., 41*, 14-22, doi:10.1016/j.jog.2005.08.013

Perez-Torrado, F. J., J. C. Carracedo, A. Rodríguez-González, V. Soler, V. R. Troll and S. Wiesmaier (2012), La erupción submarina de La Restinga en la isla de El Hierro, Canarias: Octubre 2011-Marzo 2012, *Estud. Geol., 68* (1), 5-27, doi: 10.3989/egeol.40918.179.

Riccardi U., J. Hinderer, J. P. Boy and Y. Rogister (2009), Tilt effects on GWR superconducting gravimeters, *J. Geodyn., 48* (3-5), 316-324, doi: 10.1016/j.jog.2009.09.001.

Riccardi, U., S. Rosat and J. Hinderer (2011), Comparison of the Micro-g LaCoste gPhone-054 spring gravimeter and the GWR-C026 superconducting gravimeter in Strasbourg (France) using a 300-day time series, *Metrologia, 48*, 28-39, doi: 10.1088/0026-

1394/48/1/003.

Rivera J., G. Lastras, M. Canals , J- Acosta., B. Arrese, N. Hermida, A. Micallef, O. Tello, D. Amblas, 2013, Construction of an oceanic island: Insights from the El Hierro (Canary islands) 2011–2012 submarine volcanic eruption: *Geology 41, p*. 355–358, doi:10.1130/G33863.1.

Rymer, H. and G. Williams-Jones (2000), Volcanic eruption prediction: Magma chamber physics from gravity and deformation measurements, *Geophys. Res. Lett., 27* (16), 2389-2392, doi: 10.1029/1999GL011293.

Sagiya, T., J. Barrancos, D. Calvo, E. Padrón., G. H. Hernández, P. A. Hernández, N. Pérez and J. M. P. Suárez (2012), Crustal deformation during the 2011 volcanic crisis of El Hierro, Canary Islands, Revealed by Continuous GPS Observation, *Geophys. Res. Abst., 14*, EGU2012-10243.

Sassa, K. (1935), Volcanic micro-tremors and eruption–earthquakes (Part I of the geophysical studies on the volcano Aso), *Mem. Coll. Sci., Kyoto Imp. Univ., Ser. A., 18* (5), 255-293.

Spratt, R.S. (1982). Modelling the effect of atmospheric pressure variations on gravity. *Geophysical Journal of the Royal Astronomical Society, 71*, 173–186.

Torge, W., (1989). Gravimetry. Walter de Gruyter Publishing Co.

Venedikov A. P., J. Arnoso and R. Vieira (2003), VAV: A program for tidal data processing, *Computer and Geosciences, 29* (4), 487-502, doi: 10.1016/S0098-3004(03)00019-0.

Vieira, R., M. Van Ruymbeke, J. Fernández and C. Toro (1991), The Lanzarote Underground Laboratory, *Cahiers du Centre Europeen de Geodynamique et de Seismologie, 4*, 71-86.

Wang R., F. Lorenzo-Martín and F. Roth (2006), PSGRN/PSCMP a new code for calculating

co and post-seismic deformation, geoid and gravity changes based on the viscoelastic-gravitational, *Computers and Geosciences, 32* (4), 527-541, doi: 10.1016/j.cageo.2005.08.006.

Wenzel, H.-G. (1996). The nanogal software: Earth tide data processing package ETERNA 3.30. *Bull. Inform. Marées Terrestres 124*, 9425-9439

Wenzel, H.-G. (1997). Analysis of Earth tide observations. In Wilhelm, Zürn, Wenzel (Eds.). Lecture notes in Earth Sciences. Tidal Phenomena. Springer, pp. 59-75

Zeng, X. F. and S.D. Ni (2011), Correction to "A persistent localized microseismic source near the Kyushu Island, Japan", *Geophys. Res. Lett., 38*, L16320, doi: 10.1029/2011GL048822.

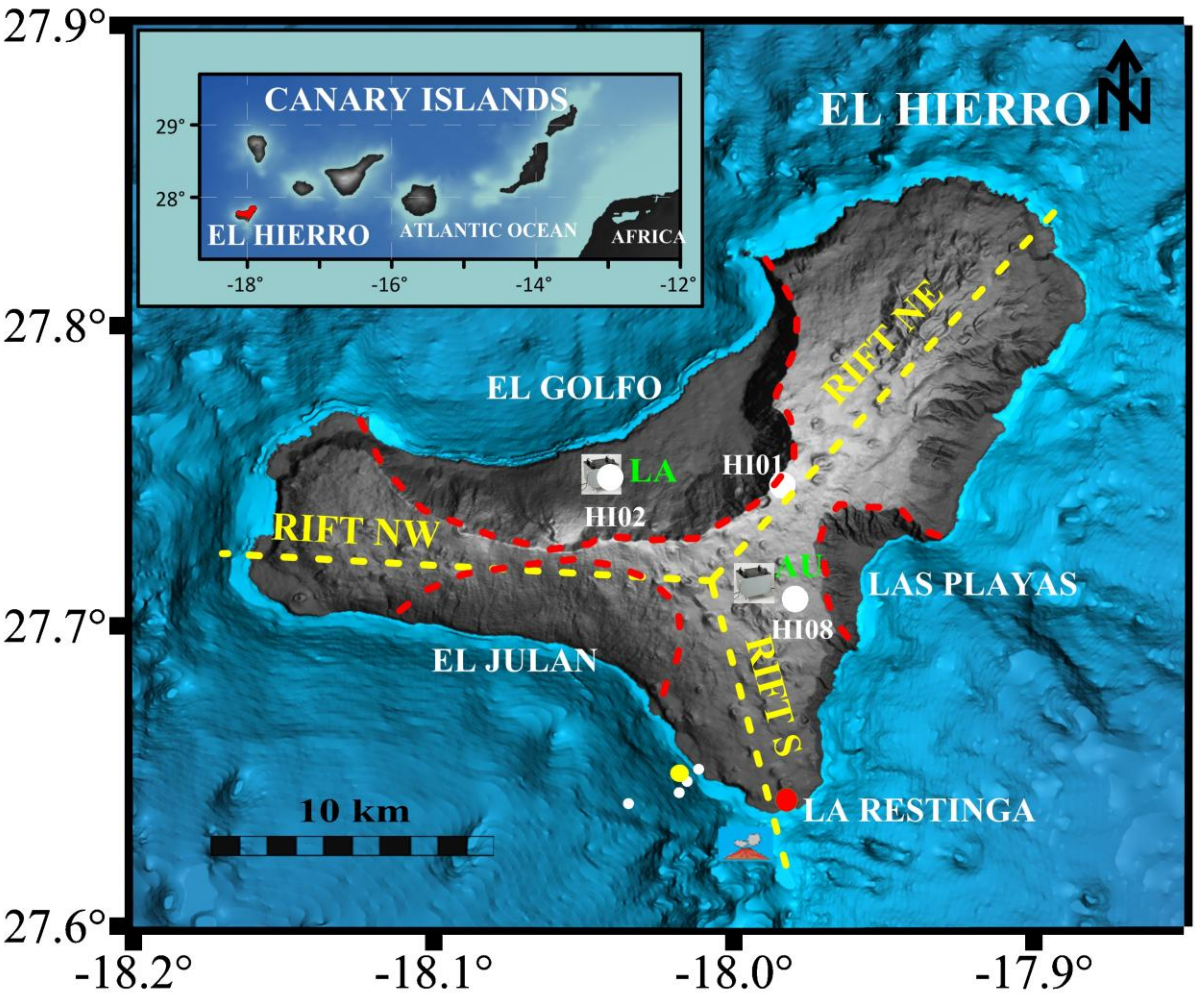

Figure 1. Relief map of El Hierro (Canary Islands) showing its main structural features (embayments of El Golfo, El Julan, and Las Playas, as well as the triple-armed volcanic rift system). The observation sites of Aula de la Naturaleza (AU) and Los Llanillos (LA) are indicated. The GPS references used are also given (HI01, HI02, HI08). The volcano icon indicates the approximate location of the submarine eruption. Small dots show the location of the seismic events of magnitude M_{bLg} > 3.6 (white color) recorded on October 7, 2011. As well, the M_{bLg} 4.3 earthquake (yellow color) of October 8, 2011, is indicated.

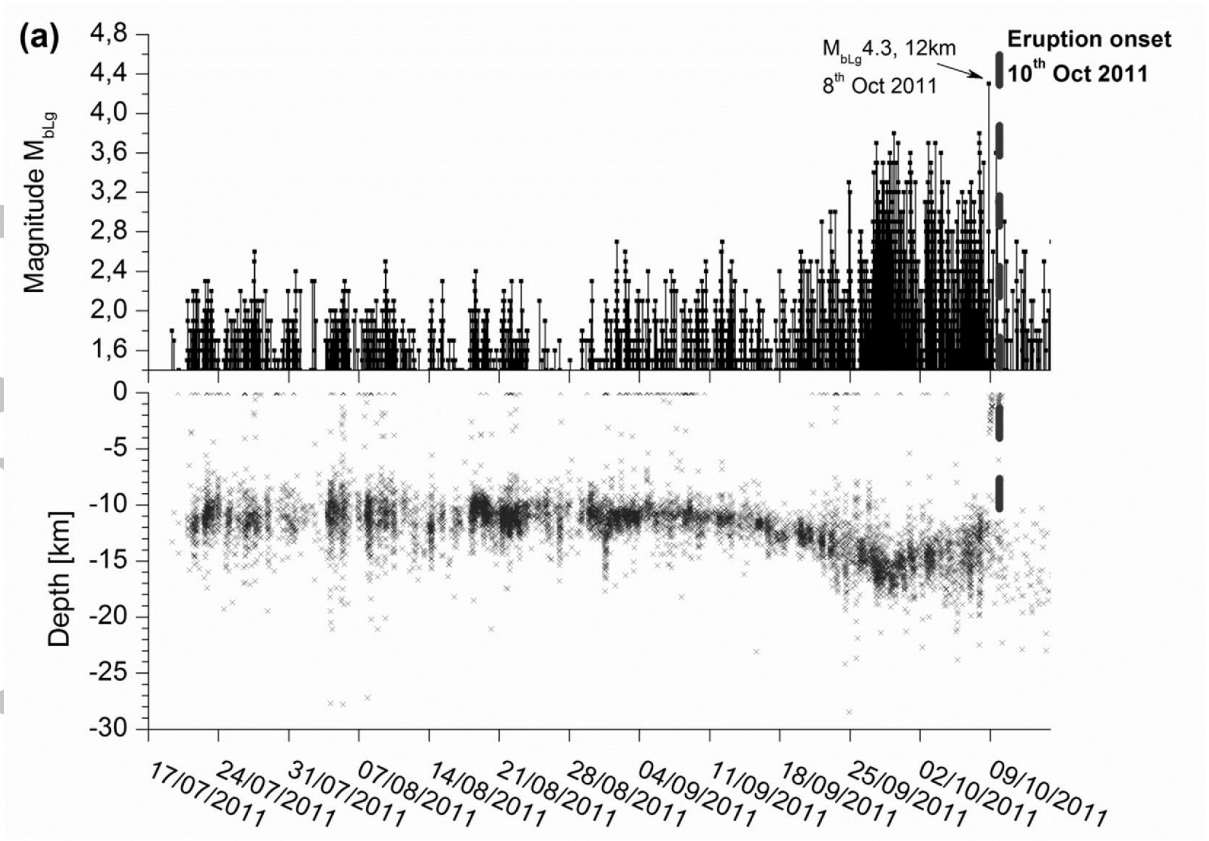

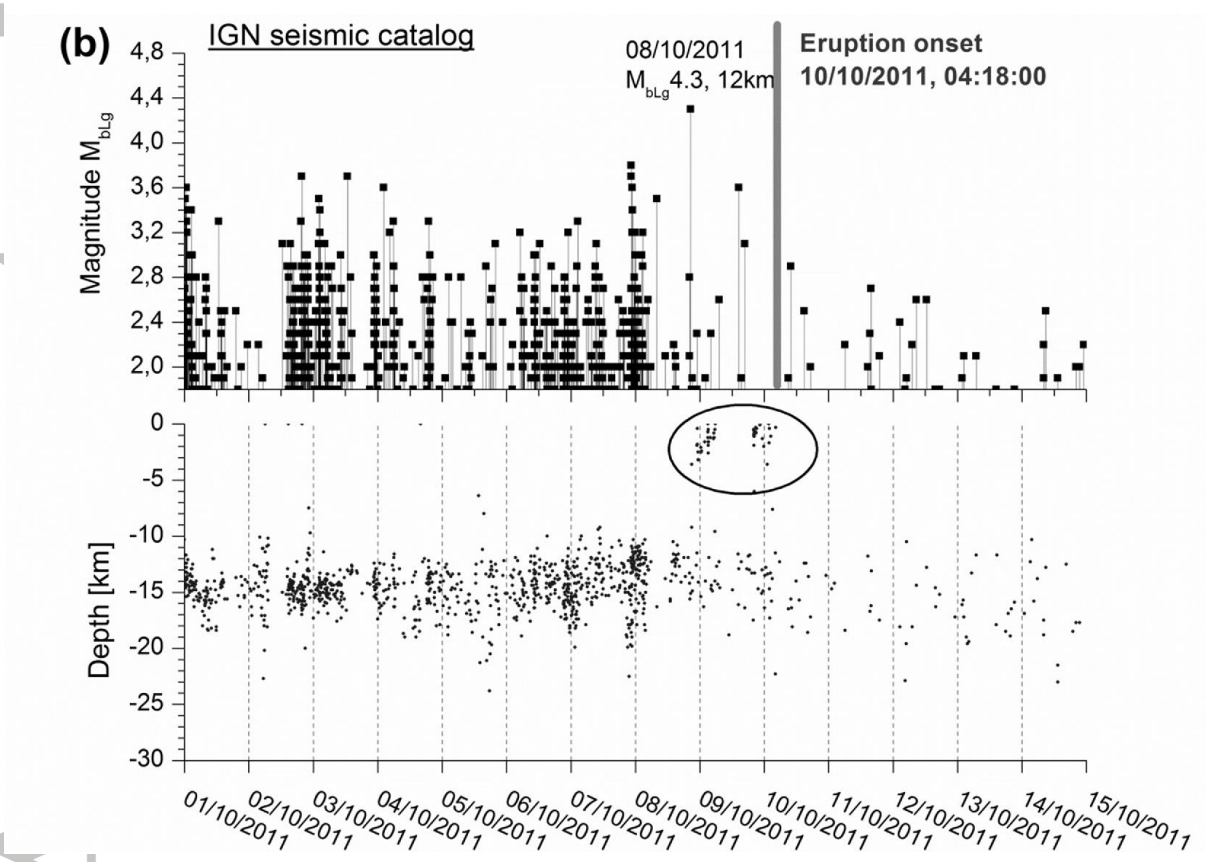

Figure 2. Magnitude and depth of the earthquakes recorded by the IGN seismic stations from the beginning of the unrest until the eruption onset (a), and a detailed view from October 1 onwards (b). The dashed line indicates the eruption onset; the shallowest earthquakes recorded before the beginning of the eruption are circled.

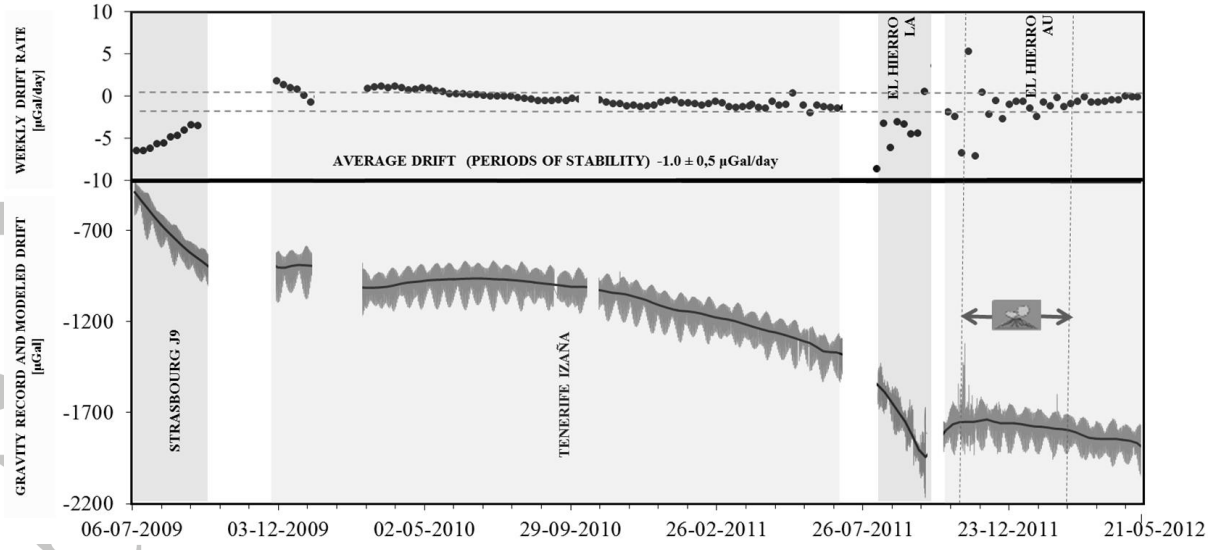

Figure 3. (Top) Weekly drift rates of the gPhone-054 gravimeter at sites in Strasbourg (France) and on Tenerife (Canary Islands, Spain) before its installation on El Hierro. Also given are the drift rates recorded by the gPhone-054 at the observation sites LA and AU from the beginning of the unrest episode on El Hierro. The dotted vertical lines indicate the period in which the tremor signal was observed at the seismic stations during the submarine eruption between October 10, 2011 and February 17, 2012. The dotted horizontal lines delimit the average instrument drift during different periods of stability. (Bottom). Raw gravity data observed at the same observing sites shown on the upper panel. The modeled instrument drift is superimposed to the observed curve.

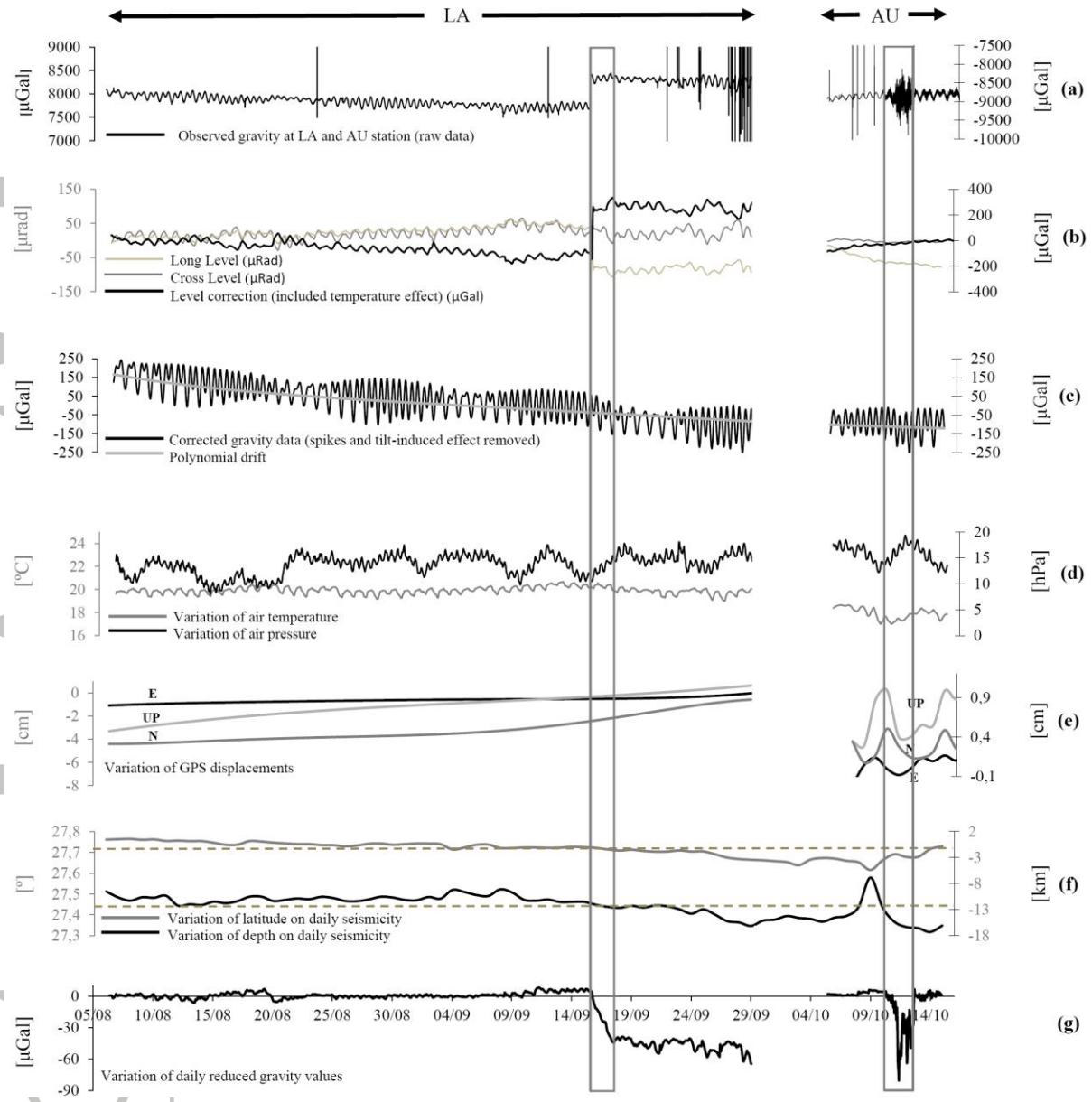

Figure 4. (a) Raw gravity data observed at LA and AU sites. (b) Signal recorded by longitudinal and transversal levels of gPhone-054. The tilt-induced (included temperature effect on the levels) gravity effect is also displayed. (c) Observed gravity data corrected from spikes and tilt-induced effects. Superimposed curve is the polynomial drift. (d) Air pressure and temperature variation observed at the respective LA and AU sites. (e) Vertical (RMS ± 0.25 cm) and horizontal (RMS ± 1.5 cm) GPS displacements measured at LA and HI08 sites, obtained through daily solutions processed in double-difference mode. (f) Variations in the depth and latitude of the earthquakes recorded by the IGN seismic stations on El Hierro Island. (g). Residual gravity (reduced for Earth and ocean tides, meteorological effects, and polar motion and tilt-induced effect) with instrument drift removed, as well as the low-pass

filtered, calculated from the gPhone-054 gravimeter records at sites LA and AU. The vertical rectangles mark the periods corresponding to the studied residual gravity anomalies. The gap after September 29 indicates the period of gPhone-054 stabilization, as it was moved to the observing site AU.

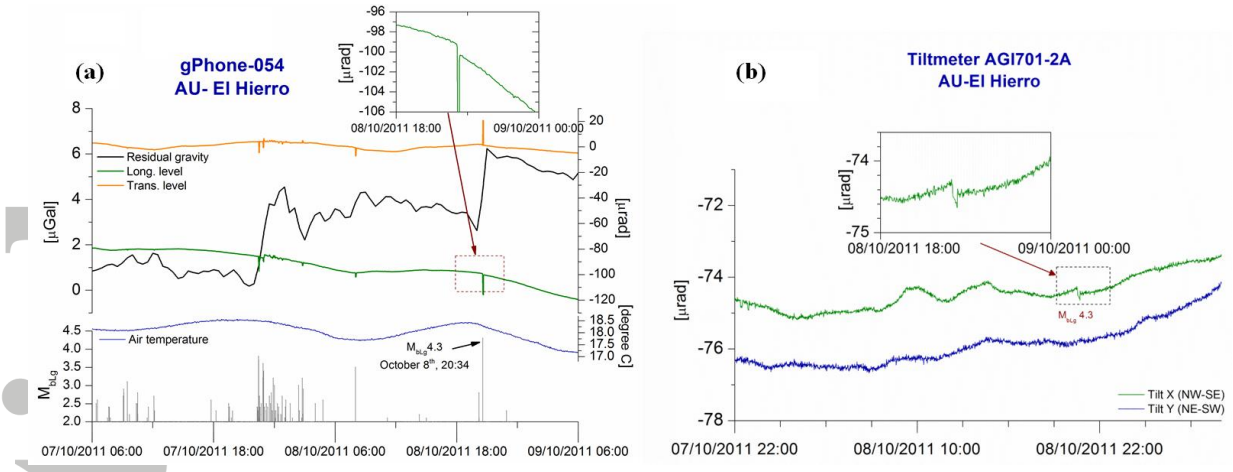

Figure 5. (a) Variation of the residual gravity, air temperature and respective tilt changes of the longitudinal (Long) and transversal (Trans) levels of the gPhone-054 during October 7-8, 2011, at site AU. The earthquakes of magnitude M_{bLg} > 2 preceding the onset of the submarine eruption are also shown. The inset zooms the Long level during the M_{bLg}4.3 event. (b) Tilts measured by biaxial AGI tiltmeter at AU during the M_{bLg} 4.3 earthquake. The inset zooms the effect of the earthquake on the X-axis.

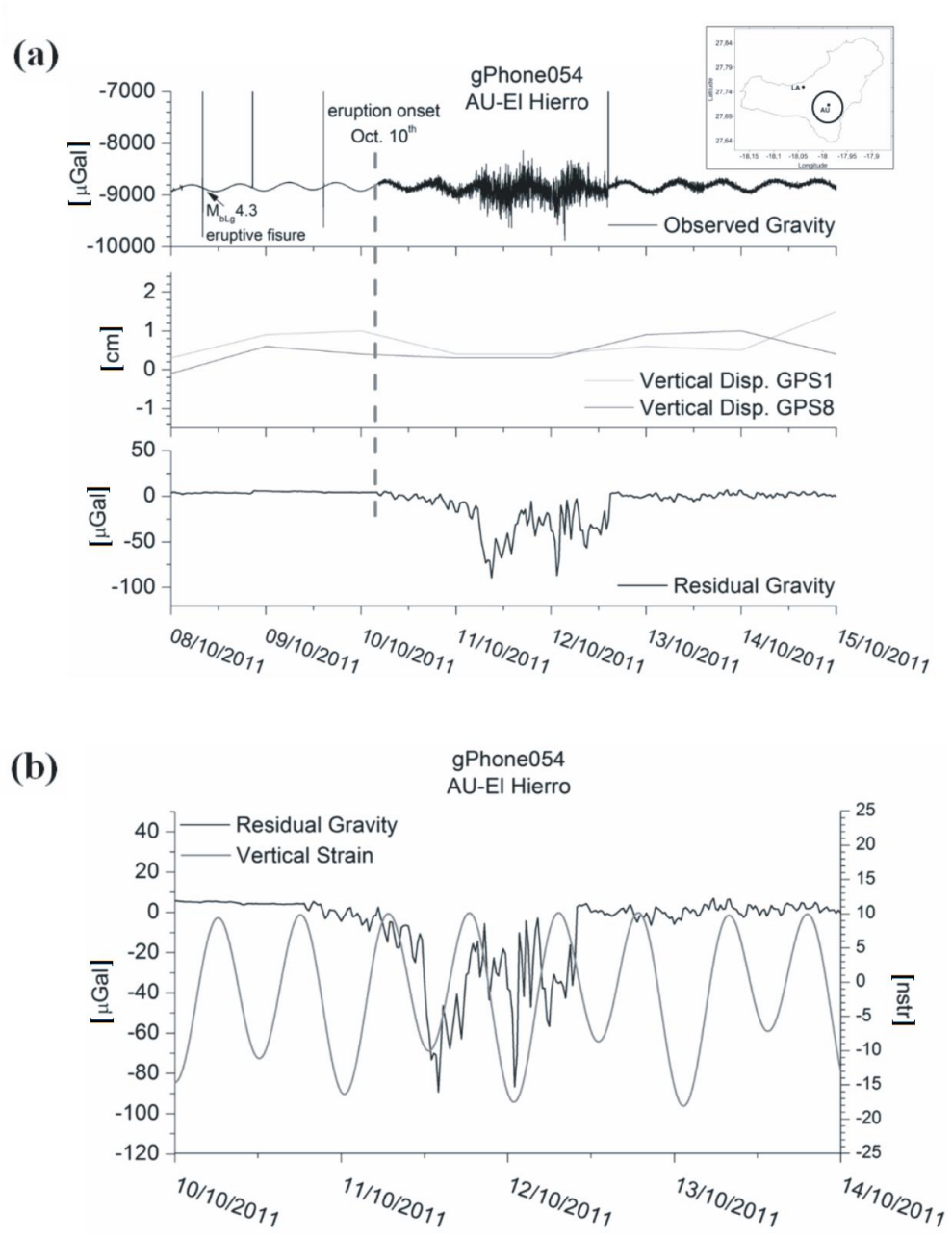

Figure 6. (a) Raw gravity sequence acquired by the gPhone-054 gravimeter at site AU on October 8–15, 2011; the gravity effect due to the volcanic tremor is clearly seen on the signal, along with the earthquake spikes. The inset shows the location of site AU (top). Vertical displacements (RMS ±0.15 cm) measured at the two nearest GPS stations (middle). Variation of the residual gravity, drift-removed and low-pass filtered at site AU (bottom). Dashed line indicates the time of the eruption onset. (b) Detailed view of the residual gravity variations on October 10–14, 2011; the body tide vertical strain (expressed in nstr, 1 nanostrain unit = 10^{-9}) computed for the same period is superimposed (see text for details).

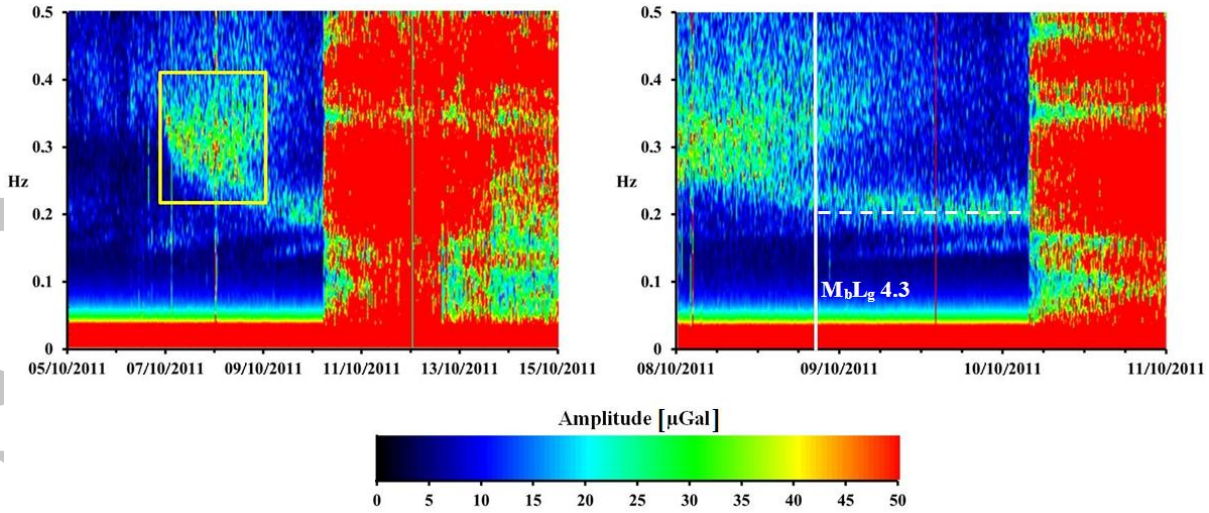

Figure 7. (Left) Moving window spectrum of high-frequency gravity signal recorded by the gPhone-054 gravimeter at site AU from September 30 to October 17, 2011. The square groups the frequency range 0.25–0.4 Hz, which was disturbed on October 6–8. (Right) Detailed view of the moving spectrum on October 8–11, showing the 0.2-Hz frequency signal (dashed line) that appeared and lasted until the beginning of the submarine eruption on October 10, date on which the volcanic tremor is clearly visible. Solid line indicates the time of the M_{bLg} 4.3 earthquake.

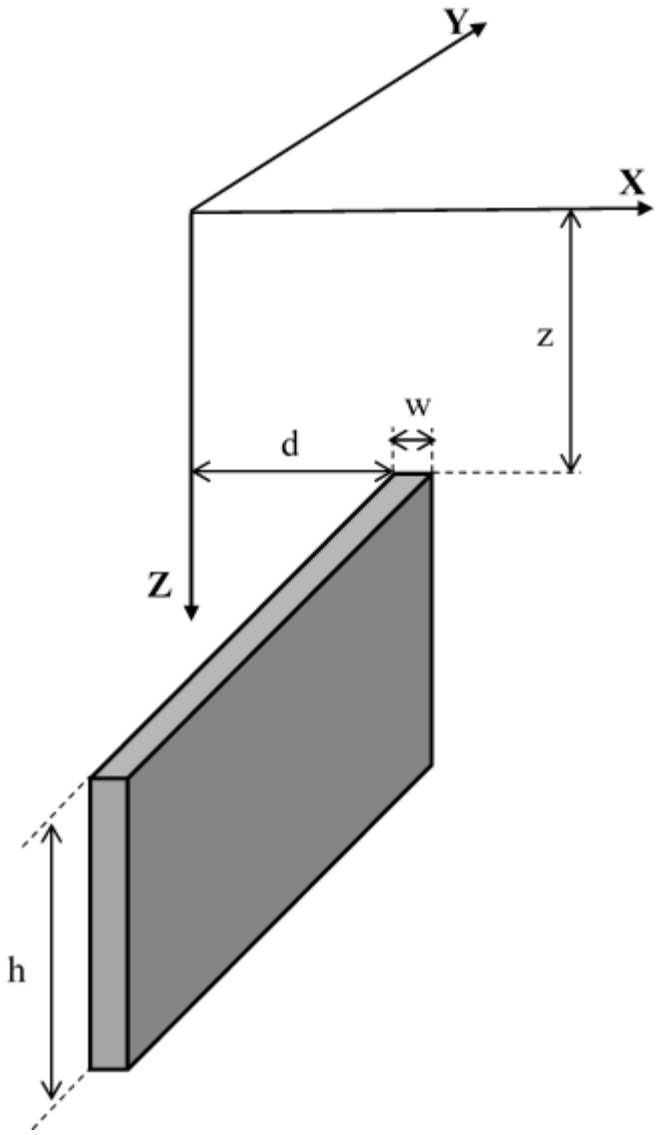

Figure 8. Geometry of a 2-D vertical sheet used to model the gravity effect produced by the eruptive fissure on October 10–13, 2011.

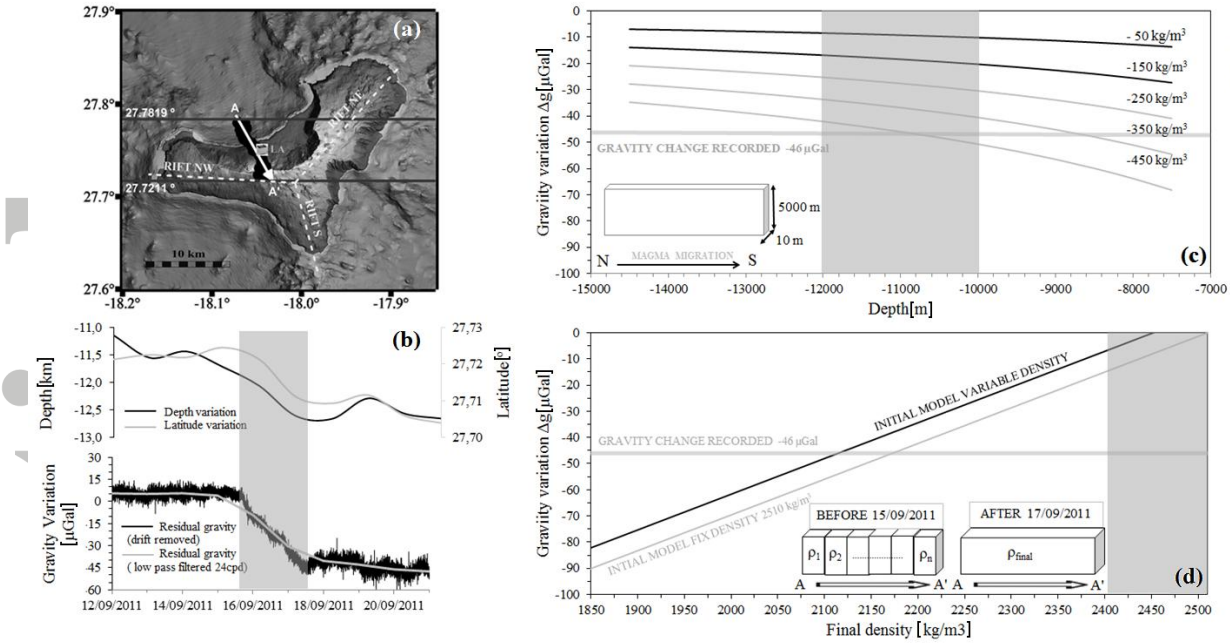

Figure 9. (a) Map of El Hierro showing the profile AA' indicating the path described by the southwards seismic migration on September 15–17, 2011. The solid horizontal lines show the latitudinal boundaries used to approach the host rock-density variation. (b) For the same period of time, (top) the variations in the depth and latitude of the earthquakes recorded by the IGN seismic stations on El Hierro, and (down) the residual gravity with drift removed, as well as low-pass filtered, calculated from the gPhone-054 gravimeter records at site LA. (c) Gravity variations as modelled by the attraction of a vertical sheet considering different density contrast values. Shadow area marks the gravity values for the depths of 10 to 12 km b.s.l. (d) The two model approaches used to describe the host rock-density variation in the calculation of the gravity attraction. The first case (top) simulates different density values for each prism taking into account the density distribution used by *Montesinos et al.* (2006). The second case (below) uses the same density value for all prisms. The inlets show the gravity attraction computed using the two host rock-density model approaches compared to the observed gravity change recorded by the gPhone-054 gravimeter at site LA on September 15–17, 2011. Shadow area marks the density values according to the modelled gravity variation.

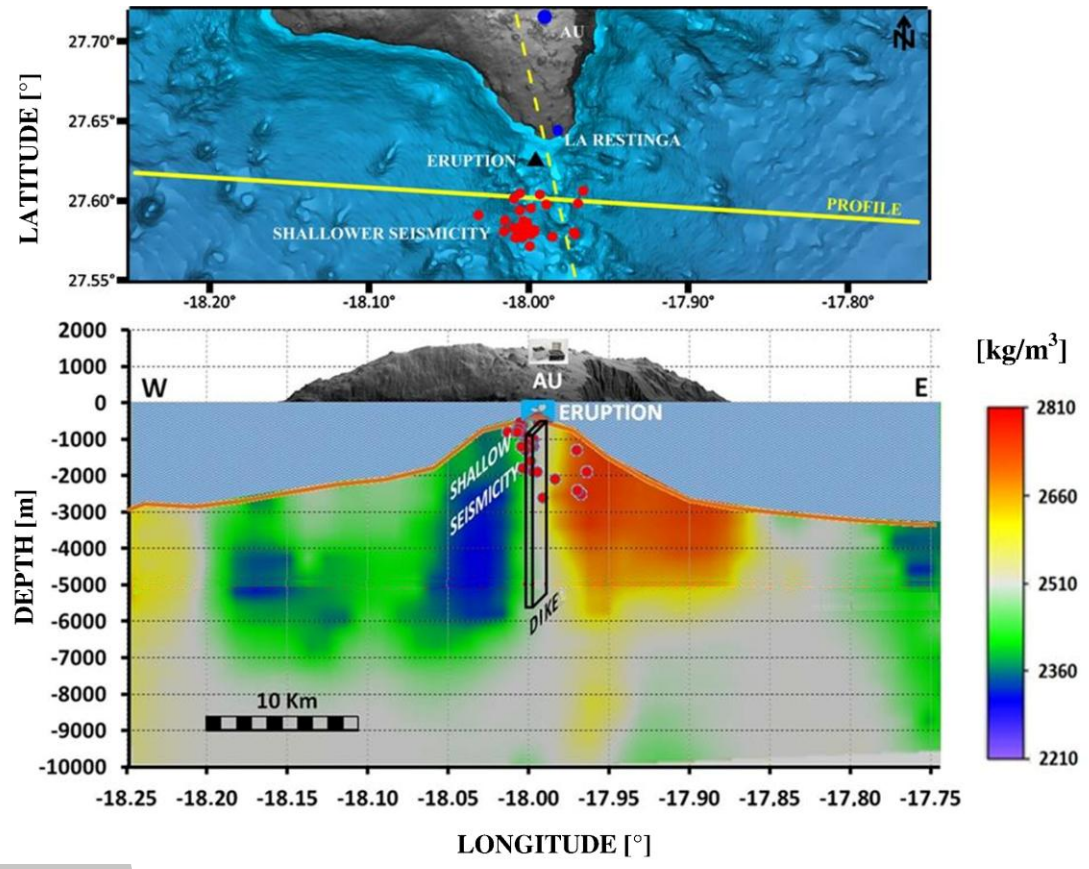

Figure 10. (Top) Detailed shaded relief map of the south of El Hierro. Observation site AU, the village of La Restinga, and the location of the submarine eruption are indicated, along with the epicenters of the shallow earthquakes (see Figure 6) before the onset of the eruption. The solid line marks the NW-SE alignment of the subsurface contrast density structures that coincides with the eruptive fracture. (Bottom) Vertical section of an E-W profile of El Hierro showing the hypocenters and differentiated high- and low-density contrast bodies based on the density contrast model of *Montesinos et al.* (2006). The dike location comes from results from this study.

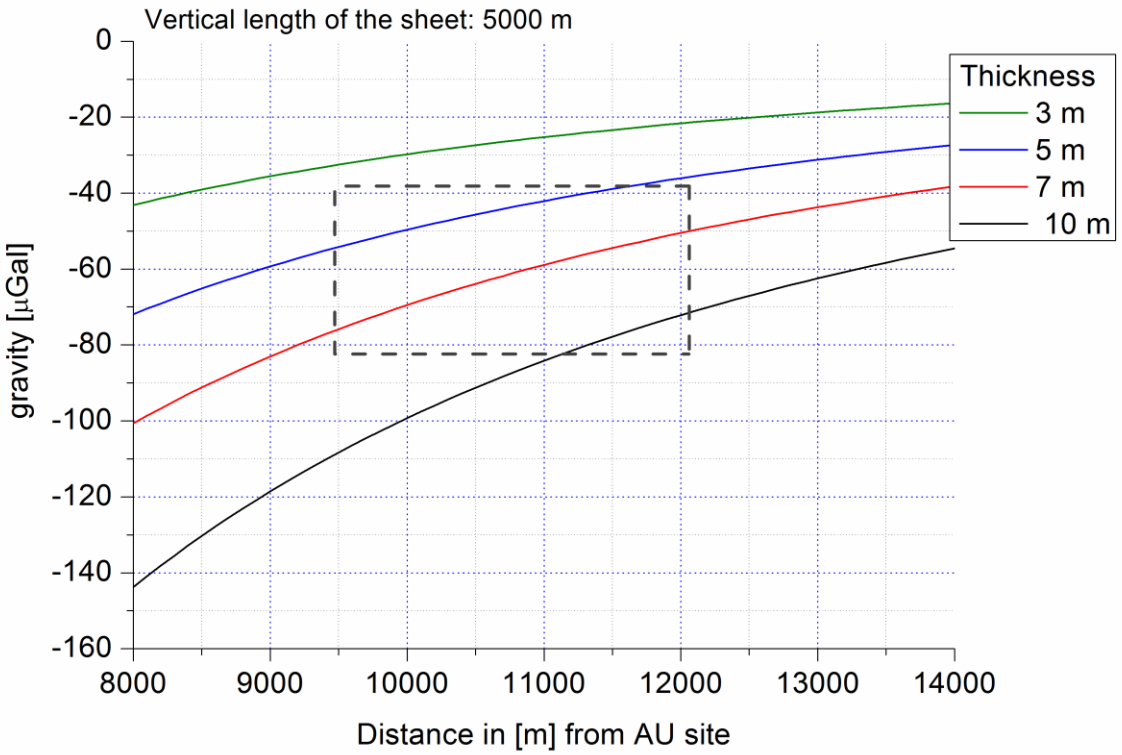

Figure 11. Gravity values computed based on the distance between site AU and the vertical sheet for different thicknesses. Values within the dashed square and for the 5–7 m thickness are most consistent with observations.

Table 1. Location of the two observing sites in El Hierro and the observation period. Geographic latitude and longitude positive in the North and East directions, respectively, and altitude referred above the sea level.

Site	Latitude (°)	Longitude (°)	Altitude (m)	Period of observation
LA	27.750	18.040	276.0	2011 08 06 – 2011 09 29
AU	27.714	17.988	950.5	20110929 -